

Authors' Response to Reviews of

The sensitivity of aerosol data assimilation to vertical profiles: case study of dust storm assimilation with LOTOS-EUROS v2.2

Mijie Pang, Jianbing Jin*, Ting Yang, Xi Chen, Arjo Segers, Batjargal Buyantogtokh, Yixuan Gu, Jiandong Li, Hai Xiang Lin, Hong Liao, and Wei Han*

RC: *Reviewers' Comment*, AR: Authors' Response, □ Manuscript Text

1. Overview

RC: *This manuscript by Pang et. al. presents a study into the sensitivity of aerosol's vertical position when assimilating ground or columnar observations. Starting from the basic formulas of the Ensemble Kalman Filter, the expected results with the two observation kinds are formulated theoretically and they are subsequently studied using a standard NWP model and real observations.*

Assimilation of this kind of observations still has many unanswered questions, and these kinds of sensitivity studies are highly relevant. I particularly enjoyed reading through the analytical formulation of the problems and then seeing actual real-world data to back up the conclusions. The manuscript is well written, with clear objectives and methodology. The drawn conclusion is fair considering the results. I wholeheartedly recommend publication after some relatively minor points are addressed. I hope the authors find the following comments useful for improving the quality of the manuscript.

AR: We would like to extend our sincere gratitude to the reviewer for the meticulous and insightful comments provided regarding our manuscript. We assure the reviewer that we have carefully considered each point raised and have made diligent efforts to address them comprehensively within the revised version of our manuscript.

2. Specific comments

RC: *As I understand it, when the authors are assimilating ground-based observations, they are not using a vertical localization scheme. By not doing this, you implicitly assume that a ground-based point measurement of concentration is representative of the whole atmospheric column, which might not hold in many cases (e.g., long range dust transport occurring at higher altitudes, local emissions near the ground measurements). The point of this manuscript is not to study localization schemes, but applying localization would eliminate the issue demonstrated in Fig. 2, panels b.1 and b.2. The text near line 205 describes what would happen with strong vertical correlations in your prior, but with localization they would diminish as you increased your distance from the point observation and reduce the problematic inflation of concentrations. I strongly recommend the authors add a case demonstrating what would happen if you used vertical localization or add a note explaining its absence.*

AR: Thanks for the comment. The vertical localization scheme is a common method to constrain the incorrect vertical correlations. We agree that applying localization would eliminate the issue of concentration inflation caused by incorrect vertical structures. While it is also the case that it may limit the correct vertical correlations to be propagated through assimilation, thus degrades the assimilation performance. We have added a note in revised manuscript and two cases that show the impact of vertical localization in Supplementary.

In addition, to test the impact of vertical localization to the assimilation performance, experiments applying EnKF with vertical localization are also carried out. It is performed on the priors of case *P-Gd-CAL* and *P-Gd-CAL*. These results can be found in the Supplementary.

Vertical localization

The vertical localization is implemented by applying a correlation coefficient into the assimilation analysis process. The correlation coefficient decreases with the increase of altitude differences between ground and the specific layer. The function is denoted as:

$$c = \exp(-3h^d) \quad (1)$$

Here, c represents the correlation coefficient and h^d is the altitude difference. As the fig. 1 shows, c decreases rapidly when h^d increases. The most noticeable decreases occur in between 100 to 1000 m. The c decreases to 0.4 when $h^d = 300$ m.

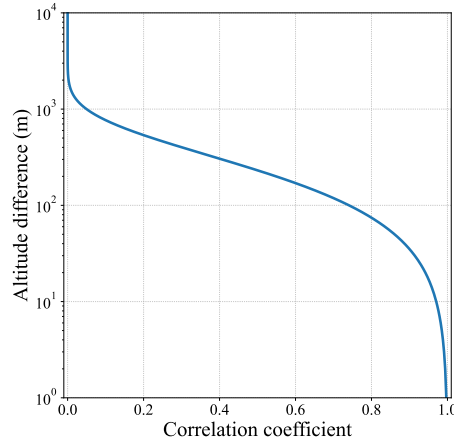


Figure 1: Relation between correlation coefficient and altitude differences. The y-axis is Logarithmized.

Impact of vertical localization

The vertical localization scheme is applied in the assimilation of case *P-Gd-CAL* and *N-Gd-CAL*. They are referred to as *P-Gd-CAL-L* and *N-Gd-CAL-L*, respectively. Figure 2 is the posterior profiles from these two cases. In the presence of correct vertical structure, through the comparison between fig. 3(d.2) and fig. 2 (a), it can be found that concentrations on ground are close to each other while the upper concentrations are closer to prior in *P-Gd-CAL-L*. This is caused by the constrain of vertical localization scheme. By the comparison of altitudinal R (in fig. 4 (a)), it can be clearly noticed that R in *P-Gd-CAL-L* decreases with altitude and becomes in line with prior above the 2 km. However, *P-Gd-CAL* continue to show improvements above the 2km. In the presence of incorrect vertical structure, it can be noticed that although the incorrect upper concentrations are not inflated much (see comparison between fig. 4(d.2) and fig. 2 (b)), it shows no improvement compared to simple EnKF (in fig. 4 (b)).

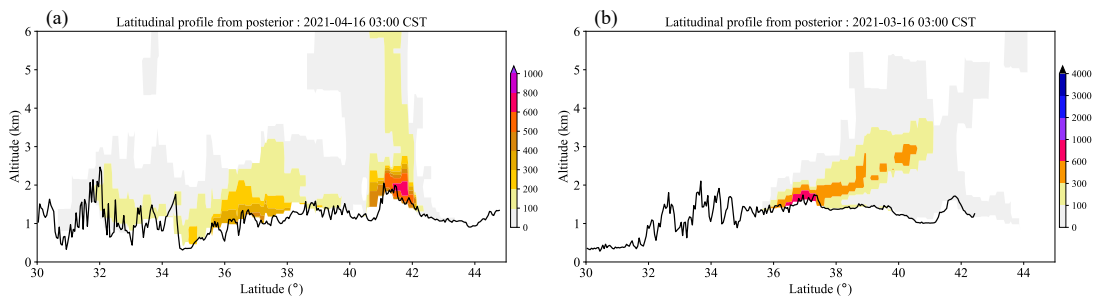


Figure 2: Dust concentration profiles following the CALIPSO scanning trajectory from the posterior of *P-Gd-CAL-L* (a) and *N-Gd-CAL-L* (b).

RC: *It would increase clarity to add a brief description about the aerosol model used in the simulations. For example, which species are used, what kind of optical properties are assumed, if there are size bins and their ranges, etc. It would also be useful to describe the observational operators for AOD and PM10 in more detail (i.e., which size bins are considered for PM10).*

AR: Thanks for the comment. Only dust particles are considered in the model. They are divided into 5 bins by diameter. Calculation of DOD follows the Mie theory. Descriptions concerning these are added in the main text and Appendix B.

All simulations commence one day prior to the initial assimilation time point, during which no dust emission occurs. The dust emission process is modeled using the *Zender03* emission parameterization scheme (Zender et al., 2003). In general, we assign the dust simulation uncertainty to the dust emission. Ensemble emission field $[\mathbf{f}_1, \dots, \mathbf{f}_N]$ are generated randomly following the emission uncertainty choice $\mathbf{f}_{\text{priori}}$ and background error covariance matrices \mathbf{B} in Jin et al. (2022). They are used to forward the LOTOS-EUROS model \mathcal{M} for the ensemble dust simulations $[\mathbf{x}_1, \dots, \mathbf{x}_N]$ as:

$$[\mathbf{x}_1, \dots, \mathbf{x}_N] = [\mathcal{M}(\mathbf{f}_1), \dots, \mathcal{M}(\mathbf{f}_N)] \quad (2)$$

Here, N refers to the total ensemble number.

DOD operator
Mie theory is applied to convert the aerosol mass concentration into AOD. It is calculated through the scatter and absorption coefficients of spherical particles with a given radius and refractive index (Gupta et al., 2018). Is defined as:

$$\tau = \sum_{k=1}^n \epsilon_d^k z^k \quad (3)$$

where τ is the simulated AOD. ϵ_d^k and z^k are the dust extinction coefficient and layer thickness at the k th layer. ϵ_d^k is calculated by the product of extinction efficiency Q_{ext} , total cross section per unit mass S ($m^2 g^{-1}$) and the aerosol mass concentration C (gm^{-3}):

$$\epsilon_d^k = Q_{ext} S C \quad (4)$$

where Q_{ext} is the sum of scattering and absorption efficiency. It's decided by the ratio of aerosol radius, incident wavelength and chemical composition (H. C., 1958). S depends on the particle size and aerosol mass density. The dust bins and diameter ranges are shown in table 1. Detailed descriptions concerning the calculation of Q_{ext} and S can be found in Section 2, Jin et al. (2023).

Table 1: Dust size bins and diameter ranges

Bins	dust_ff	dust_f	dust_ccc	dust_cc	dust_c
Diameter range (μm)	0.01-1	1-2.5	2.5-4	4-7	7-10

RC: *In the case studies, it is mentioned that DOD is assimilated from Himawari. Does this mean that only dust is considered in the model AOD operator? Maybe it can be referred to as a "DOD operator" for clarity.*

AR: Thanks for the comment. It is true that only dust is considered in the model AOD operator. "DOD operator" is more clarified and it is replaced in the revised manuscript.

RC: *When comparing with CALIPSO, is the CALIOP aerosol classification checked to ensure that dust dominated the scenes? There are methods for extracting the dust-only component from lidar measurements (for example, Mamouri et. al. 2017 and Amiridis et. al. 2015), which might be useful, given that the model also only includes desert dust in the extinction profiles.*

AR: Thanks for the comment. We have adopted the method in Mamouri and Ansmann (2017) to classify the dust in the total extinction coefficient. The depolarization ratio profile data from CALIOP products is used to distinguish the dust from total particles.

CALIOP dust classification

The polarization lidar–photometer networking (POLIPHON) technology was applied to classify dust and non-dust aerosol components and to estimate the fine and coarse dust contributions to the overall backscatter and extinction coefficients and particle mass concentration (Mamouri and Ansmann, 2014, 2017). The method is solely based on the use of characteristic depolarization ratios for fine dust, coarse dust, and non-dust aerosol.

The dust backscatter coefficient β_d is calculated by:

$$\beta_d = \begin{cases} \beta_p & \delta_p \geq \delta_d \\ \beta_p \frac{(\delta_p - \delta_{nd})(1 + \delta_d)}{(\delta_d - \delta_{nd})(1 + \delta_p)} & \delta_{nd} < \delta_p < \delta_d \\ 0 & \delta \leq \delta_{nd} \end{cases} \quad (5)$$

where δ_p , δ_d and δ_{nd} are the depolarization ratio of total particle, dust (fine+coarse) and non-dust, respectively. β_p is the particle backscatter coefficient. For reference, δ_d is set to be 0.31 under the wavelength of 532 nm. And δ_{nd} is assumed to be 0.05. From this equation we can tell that δ_p greater than δ_d means that the dust dominates the total particles.

The coarse dust backscatter coefficient β_{dc} is obtained by the following equation:

$$\beta_{dc} = \begin{cases} \beta_p & \delta_p \geq \delta_{dc} \\ \beta_p \frac{(\delta_p - \delta_{nd+df})(1 + \delta_{dc})}{(\delta_{dc} - \delta_{nd+df})(1 + \delta_p)} & \delta_{nd+df} < \delta_p < \delta_{dc} \\ 0 & \delta \leq \delta_{nd} \end{cases} \quad (6)$$

Here, δ_{dc} is the coarse dust depolarization ratio and δ_{nd+df} is the depolarization ratio of mixture of non-dust and fine dust particles. δ_{df} and δ_{dc} are estimated to be 0.16 ± 0.02 and 0.37 ± 0.03 , respectively under the wavelength of 532 nm.

Figure 3 shows the depolarization ratio profiles in correspondence to the 4 cases in the manuscript. Values greater than 0.31 are assigned as red. By comparison with the extinction coefficient profiles, the depolarization ratio profiles show that the dust is the dominant particle in these 4 cases.

RC: *When comparing CALIPSO to the model, some statistics would be interesting (e.g. RMSE). Currently the comparison is “by eye”.*

AR: Thanks for the comment. We have calculated the correlation coefficient (R) across the altitude and latitude as the evaluation metric. To align different vertical resolutions between model and CALIPSO observations, concentration fields from model are linear interpolated into the CALIPSO data point. Metrics on all cases are calculated. Figures and descriptions are added in the Supplementary. Note that these metrics are calculated by paired data. It can be biased for the high missing rate of CALIPSO profile.

Statistical evaluation

Figures 4 and 5 are the altitudinal and latitudinal trend of correlation coefficient (R) between concentration fields and CALIPSO observations. The fields are linear interpolated into the CALIPSO data point. These data are paired within the altitudinal and latitudinal direction. In the case of *P-Gd-CAL* and *N-Gd-CAL*, as shown in figs. 4 and 5 (a,b), it can be noticed that ground data assimilation can optimize the dust field under the correct vertical structure. Improvements of R can be seen in the 1st case. Meanwhile, as figs. 4 and 5 (b) shows, it can also maintain the incorrect vertical structure. In the case of DOD assimilation, similar trend is shown. The incorrect vertical structure remains after assimilation. Moreover, there is a noticeable degrade of R found in fig. 5 (c), which is in line with the

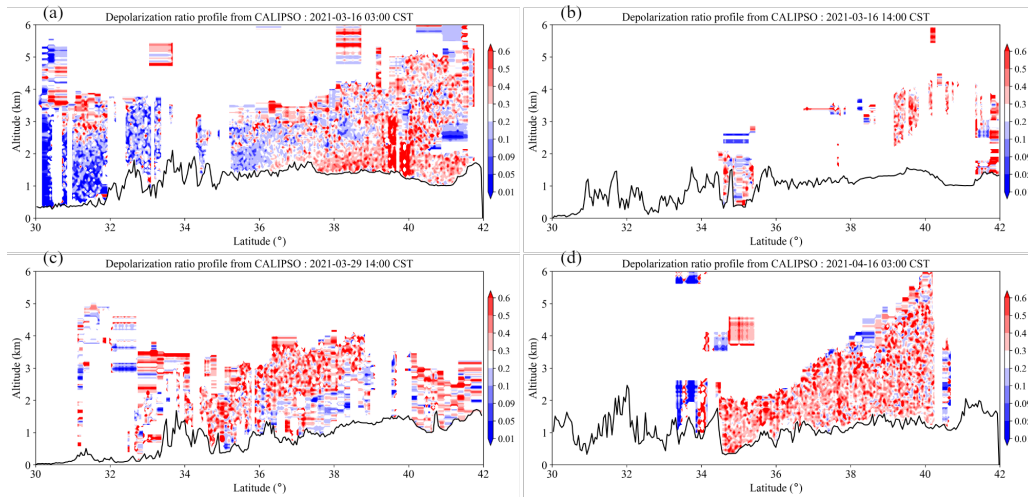


Figure 3: Depolarization ratio profiles from CALIOP for the correspondent 4 cases.

inflated incorrect dust structure in *NP-DOD-CAL*.

RC: *In the introduction, it would be helpful to mention uncertainties in optical properties when discussing the difficulties in assimilating aerosol-related observations (around line 50). Some of the publications mentioned in section 2.3.1 about LiDAR assimilation would fit in the introduction as well, around line 70.*

AR: Thanks for the comment. Corresponding references are added.

In perspective of aerosol data assimilation, the main object is to reproduce the optimal aerosol states (Liu et al., 2011), concerning their spatial, vertical, aerosol species and size distribution features. While the available observations commonly measure their mixed state. For example, AOD that is column-integrated optical extinction of all aerosols and high uncertainties exist in the optical properties of aerosol (Tsikerdekis et al., 2021). Ground PM₁₀ concentration measurement that is additive sum of all particles with diameter less than 10 μm. They are not directly comparable to the aerosol state.

While in reality, the ground stations produce scattered concentrations on ground, satellite and LiDAR receive column-integrated information about the aerosol or a single profile once a day (Sekiyama et al., 2010; Hofer et al., 2017; Cheng et al., 2019; Escribano et al., 2022).

RC: *Line 69 mentions that no instrument can provide continuous vertical information about aerosols, but both ground-based and space-borne LiDARs do that. They do not provide 3D fields, but the information is continuous.*

AR: Thanks for the comment. We intended to mean that no instrument can fulfill 1) continuous, 2) vertical, 3) large and consistent spatial coverage at the same time. The original description is inadequate and it has been adapted as:

While in reality, the ground stations produce scattered concentrations on ground, satellite and LiDAR receive column-integrated information about the aerosol or a single profile once a day (Sekiyama et al., 2010; Hofer et al., 2017; Cheng et al., 2019; Escribano et al., 2022). None of them can provide a continuous vertical information about the aerosol with large spatial coverage.

RC: *Please consider providing more information about the modelling setup to aid in the reproduction of your experiments. More details could be added to section 2.1.1 about model settings and what kind of initial and boundary conditions are used. Consider uploading configuration files and IC/BC files to a public repository.*

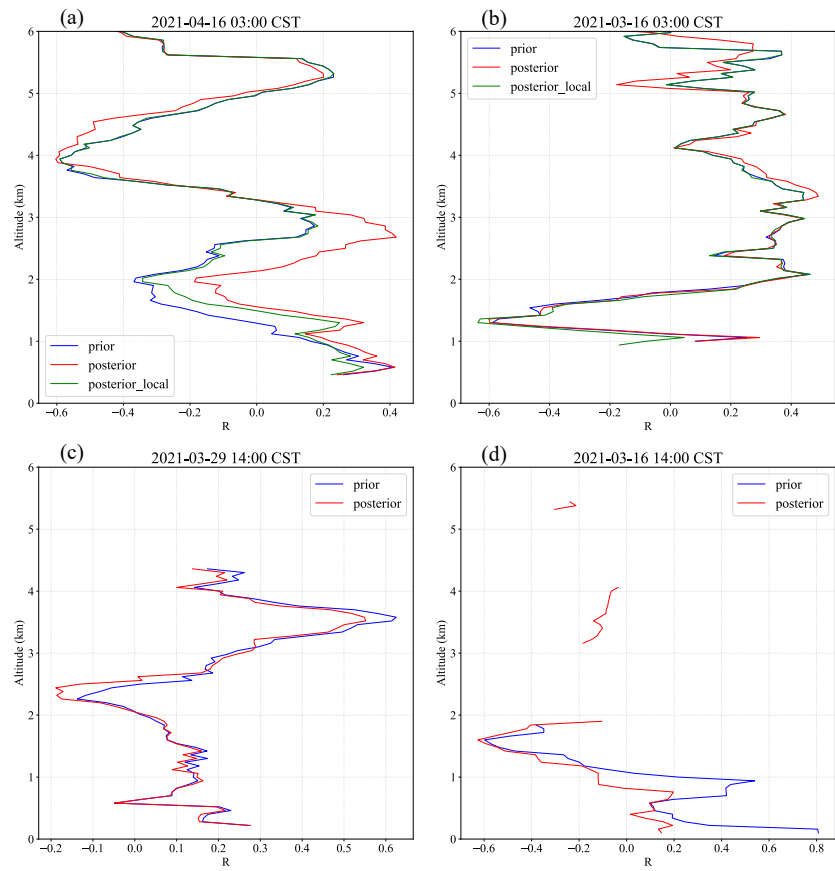


Figure 4: The correlation coefficient averaged on different altitudes. Each altitude contains all the paired data points (Concentration and extinction coefficient) along with the CALIPSO scan line

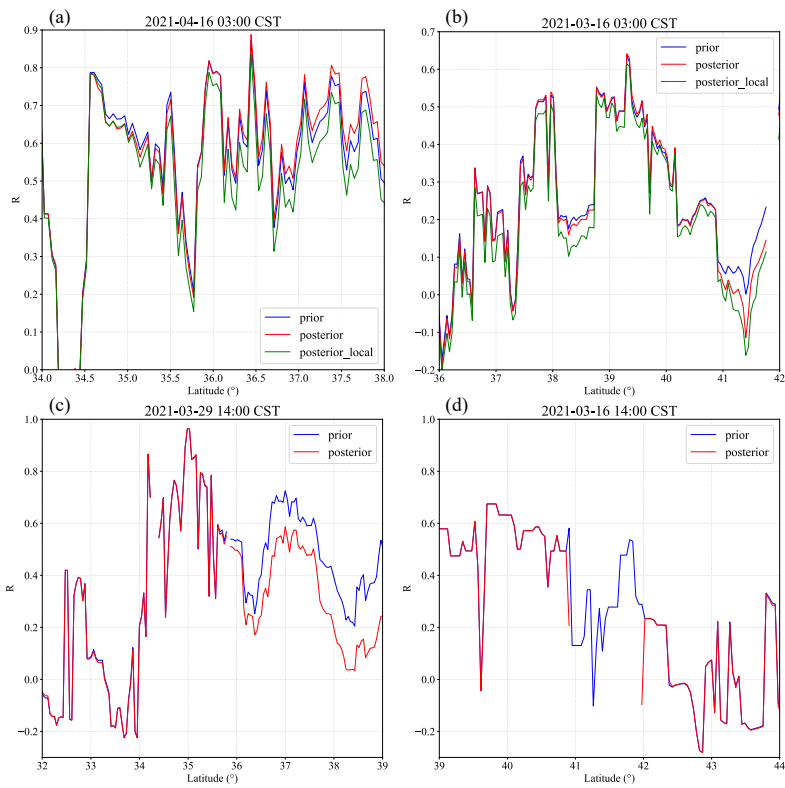


Figure 5: The correlation coefficient averaged on different latitudes. Each latitude contains all the paired data points (Concentration and extinction coefficient) along with the CALIPSO scan line

AR: Thanks for the comment. More descriptions concerning the model setup are added in the revised manuscript. Initial state files and analysis files are uploaded to Zenodo. Concerning links are added in the manuscript:

LOTOS-EUROS

The LOTOS-EUROS v2.2 is used to simulate the dust aerosol. The LOTOS-EUROS model is a 3D chemistry transport model aimed for air quality forecasting (Manders et al., 2017). It has also been applied in source apportionment and emission inversion worldwide. In this study, The modeling domain spans from 15° N to 50° N and from 70° E to 140° E with spatial resolution of $0.25^\circ \times 0.25^\circ$. Vertically, it comprises 21 layers with a top level at 10 km, which is adequate for recognizing the vertical structure. 3 hourly ECMWF operational forecast is used to drive the model. The boundary conditions are set to zero assuming that all the dust aerosols are emitted during the simulation window. Dust aerosol processes including emission, advection, diffusion, deposition and sedimentation are considered in the model.

All simulations commence one day prior to the initial assimilation time point, during which no dust emission occurs. The dust emission process is modeled using the *Zender03* emission parameterization scheme (Zender et al., 2003). In general, we assign the dust simulation uncertainty to the dust emission. Ensemble emission field $[f_1, \dots, f_N]$ are generated randomly following the emission uncertainty choice f_{priori} and background error covariance matrices B in Jin et al. (2022). They are used to forward the LOTOS-EUROS model \mathcal{M} for the ensemble dust simulations $[x_1, \dots, x_N]$ as:

$$[x_1, \dots, x_N] = [\mathcal{M}(f_1), \dots, \mathcal{M}(f_N)] \quad (7)$$

Here, N refers to the total ensemble number.

The ensemble initial fields, prior and posterior fields used in this paper are archived in <https://doi.org/10.5281/zenodo.14846965>.

3. Technical Comments

RC: *At lines 148-149, the superscripts 'a' and 'f' are used, probably referring to analysis and forecast. This should be mentioned for clarity.*

AR: Thanks for the comment. The superscripts 'a' and 'f' do mean the analysis and forecast. They are clarified in the manuscript as below:

EnKF is a Monte Carlo approach based on Kalman filter theory. EnKF maintains a set of model states to approximate the probability distribution of the model state or parameter. It includes the forecast step and the analysis step. In the forecast step, each posterior ensemble member $x_{t-1}^{a,i}$ at previous time $t - 1$ is integrated forward according to the model dynamics \mathcal{M} to generate a prior forecast $x_t^{f,i}$ at the next moment t . i refers to the ensemble member here.

$$x_t^{f,i} = \mathcal{M}(x_{t-1}^{a,i}) \quad (8)$$

RC: *Line 176 includes the phrase "[...] to nudge the 3D states [...]". Since nudging refers to a specific family of methods, it might be clearer to use another word here.*

AR: Thanks for the comment. It has been replaced as "optimize" here.

In practice, each of the PM_{10} observations could be assimilated to optimize the 3D states that are correlated.

RC: *In Figure 5, it would be interesting to see the ground-based LiDAR profiles as a third line in the bottom panel, for direct comparison with the model. I understand that the model plots show concentration, but they could also be extinction, since that is a required step for computing the AOD/DOD.*

AR: Thanks for the comment. We have inserted the extinction coefficient from the ground LiDAR into the bottom panel. Although they are not directly comparable, positive correlation exists between them especially when only dust particles are considered in this study. It's easier to tell the difference of structure when they are plotted together.

Figure 6 (b) illustrates the hourly prior and posterior dust profile during the selected period. The profiles of extinction coefficient are also plotted in blue dash dot line. The x-axis which represents concentrations is logarithmic rescaled here. In terms of prior profiles, dust loading have extended up to 5 km at 8:00 and declined to 3 km at 16:00. This structure is inconsistent with the LiDAR profile, in which time only little dust was observed. The dust storm has been overestimated to a large extent in height. The ground aerosol concentrations are lower than $200 \mu\text{g m}^{-3}$ throughout eight time points, which are much lower than the observations (over $1000 \mu\text{g m}^{-3}$). After assimilation, this underestimation has been mitigated. The ground dust concentrations are amplified several times to better fit the observations. Meanwhile, the erroneous vertical structure is also intensified in the first six moments, as can clearly seen in the comparison between concentration and extinction coefficient. Especially in 9:00, the dust loading above 2 km have been amplified to over $1000 \mu\text{g m}^{-3}$, which will give out utterly incorrect information about the dust storm structure and impact the further forecasting.

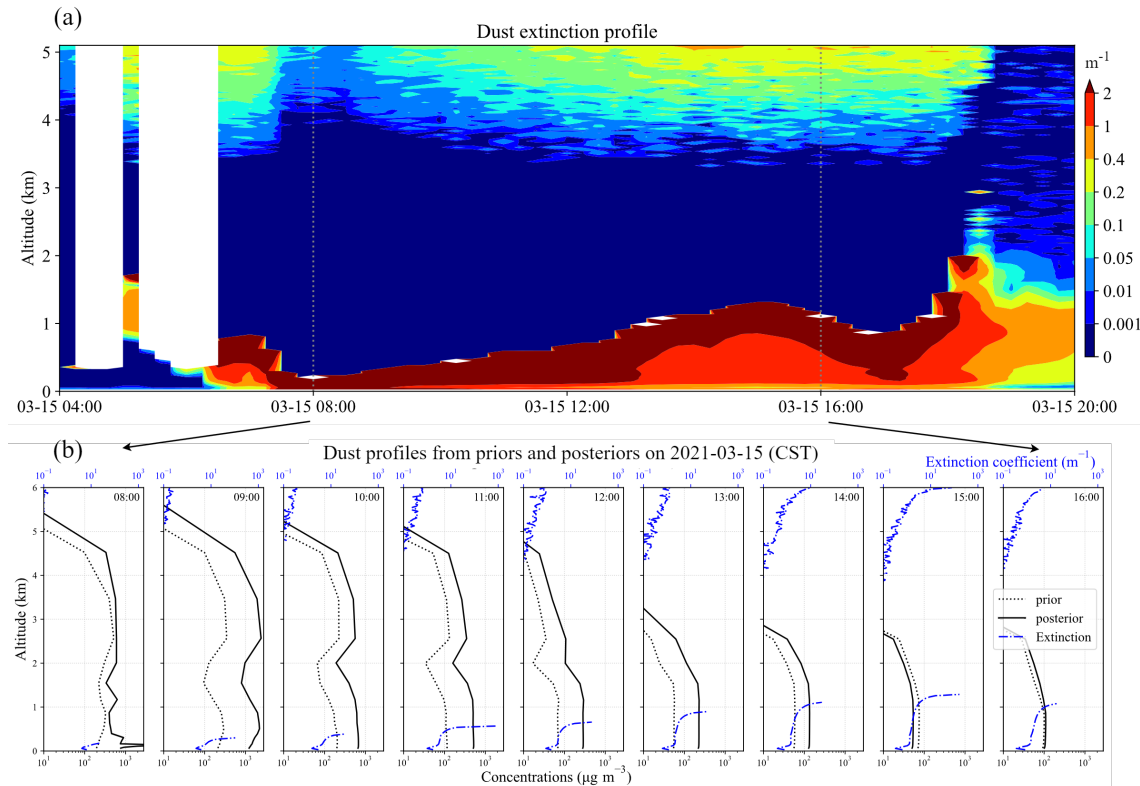


Figure 6: Time series of dust extinction coefficient profile obtained from LiDAR (a). The assimilation analysis is performed hourly from 8:00 to 16:00. Figure below is hourly dust profile line from prior (dash line) and posterior (solid line) (b). The extinction coefficient is also plotted (blue dash dot line). The profile data is extracted from the closest grid point to the LiDAR location. The x-axis is logarithmic rescaled. Note that instead of using the posterior in previous time to propagate the model, analysis here is separately conducted on the static background.

RC: *Lines 374-375, I believe the observations have 'low/high dimensionality'*

AR: Thanks for the correction. The observation is a process instead of a state. Hence, 'dimensionality' is not suitable to describe it. We have corrected these statements throughout the revised paper.

However, challenges persist in reconciling these observations with the model's high-dimensional state.

- RC:** *At various points in the manuscript, the word “fraud” is used in regard to low quality observations or information. I think this specific word implies malicious intent, which I hope is not true in any case. For example, line 70 would be clearer as “When there is incorrect/inaccurate information [...]” instead of “When there is fraud information [...]”. Consider replacing all instances of “fraud” with something milder.*
- AR:** Thanks for the comment. The usage of "fraud" does imply some malicious intent. It has been replaced by "incorrect" across the manuscript.

References

- Cheng, Y., Dai, T., Goto, D., Schutgens, N. A. J., Shi, G., and Nakajima, T.: Investigating the Assimilation of CALIPSO Global Aerosol Vertical Observations Using a Four-Dimensional Ensemble Kalman Filter, *Atmos. Chem. Phys.*, 19, 13 445–13 467, , 2019.
- Escribano, J., Di Tomaso, E., Jorba, O., Klose, M., Gonçalves Ageitos, M., Macchia, F., Amiridis, V., Baars, H., Marinou, E., Proestakis, E., Urbanneck, C., Althausen, D., Bühl, J., Mamouri, R.-E., and Pérez García-Pando, C.: Assimilating Spaceborne Lidar Dust Extinction Can Improve Dust Forecasts, *Atmos. Chem. Phys.*, 22, 535–560, , 2022.
- Gupta, M. C., Ungaro, C., Foley, J. J., and Gray, S. K.: Optical Nanostructures Design, Fabrication, and Applications for Solar/Thermal Energy Conversion, *Solar Energy*, 165, 100–114, , 2018.
- H. C., v. d. H.: Light Scattering by Small Particles. By H. C. van de Hulst. New York (John Wiley and Sons), London (Chapman and Hall), 1957. Pp. Xiii, 470; 103 Figs.; 46 Tables. 96s, *Quarterly Journal of the Royal Meteorological Society*, 84, 198–199, , 1958.
- Hofer, J., Althausen, D., Abdullaev, S. F., Makhmudov, A. N., Nazarov, B. I., Schettler, G., Engelmann, R., Baars, H., Fomba, K. W., Müller, K., Heinold, B., Kandler, K., and Ansmann, A.: Long-Term Profiling of Mineral Dust and Pollution Aerosol with Multiwavelength Polarization Raman Lidar at the Central Asian Site of Dushanbe, Tajikistan: Case Studies, *Atmos. Chem. Phys.*, 17, 14 559–14 577, , 2017.
- Jin, J., Pang, M., Segers, A., Han, W., Fang, L., Li, B., Feng, H., Lin, H. X., and Liao, H.: Inverse Modeling of the 2021 Spring Super Dust Storms in East Asia, *Atmos. Chem. Phys.*, 22, 6393–6410, , 2022.
- Jin, J., Henzing, B., and Segers, A.: How Aerosol Size Matters in Aerosol Optical Depth (AOD) Assimilation and the Optimization Using the Ångström Exponent, *Atmos. Chem. Phys.*, 23, 1641–1660, , 2023.
- Liu, Z., Liu, Q., Lin, H.-C., Schwartz, C. S., Lee, Y.-H., and Wang, T.: Three-Dimensional Variational Assimilation of MODIS Aerosol Optical Depth: Implementation and Application to a Dust Storm over East Asia, *J. Geophys. Res.*, 116, , 2011.
- Mamouri, R. E. and Ansmann, A.: Fine and Coarse Dust Separation with Polarization Lidar, *Atmos. Meas. Tech.*, 7, 3717–3735, , 2014.
- Mamouri, R.-E. and Ansmann, A.: Potential of Polarization/Raman Lidar to Separate Fine Dust, Coarse Dust, Maritime, and Anthropogenic Aerosol Profiles, *Atmos. Meas. Tech.*, 10, 3403–3427, , 2017.
- Manders, A. M. M., Builtjes, P. J. H., Curier, L., Denier van der Gon, H. A. C., Hendriks, C., Jonkers, S., Kranenburg, R., Kuenen, J. J. P., Segers, A. J., Timmermans, R. M. A., Visschedijk, A. J. H., Wichink Kruit, R. J., van Pul, W. A. J., Sauter, F. J., van der Swaluw, E., Swart, D. P. J., Douros, J., Eskes, H., van Meijgaard, E., van Ulf, B., van Velthoven, P., Banzhaf, S., Mues, A. C., Stern, R., Fu, G., Lu, S., Heemink, A., van Velzen, N., and Schaap, M.: Curriculum Vitae of the LOTOS–EUROS (v2.0) Chemistry Transport Model, *Geosci. Model Dev.*, 10, 4145–4173, , 2017.

- Sekiyama, T. T., Tanaka, T. Y., Shimizu, A., and Miyoshi, T.: Data Assimilation of CALIPSO Aerosol Observations, *Atmos. Chem. Phys.*, 10, 39–49, , 2010.
- Tsikerdekis, A., Schutgens, N. A. J., and Hasekamp, O. P.: Assimilating Aerosol Optical Properties Related to Size and Absorption from POLDER/PARASOL with an Ensemble Data Assimilation System, *Atmos. Chem. Phys.*, 21, 2637–2674, , 2021.
- Zender, C. S., Bian, H., and Newman, D.: Mineral Dust Entrainment and Deposition (DEAD) Model: Description and 1990s Dust Climatology, *J. Geophys. Res.*, 108, , 2003.